Research Square

Preprints are preliminary reports that have not undergone peer review.
They should not be considered conclusive, used to inform clinical practice,
or referenced by the media as validated information.

β-amyloid monomer scavenging by an anticalin protein prevents neuronal hyperactivity

Benedikt Zott (benedikt.zott@tum.de)
Technical University of Munich https://orcid.org/0000-0003-4537-7381
Lea Nästle
Technical University of Munich
Christine Grienberger
Brandeis University
Manuel Knauer
Technical University of Munich
Felix Unger
Technical University of Munich
Aylin Keskin
Technical University of Munich
Anna Feuerbach
Technical University of Munich
Marc Aurel Busche
University College London https://orcid.org/0000-0002-4416-7553
Arne Skerra
Technical University Munich https://orcid.org/0000-0002-5717-498X
Arthur Konnerth
Technical University of Munich https://orcid.org/0000-0002-9548-2676

Article

Keywords:

Posted Date: February 3rd, 2023

DOI: https://doi.org/10.21203/rs.3.rs-2514083/v1

License: This work is licensed under a Creative Commons Attribution 4.0 International License.
Read Full License

Abstract

Hyperactivity mediated by synaptotoxic β-amyloid (Aβ) oligomers is one of the earliest forms of neuronal dysfunction in Alzheimer's disease. In the search for a preventive treatment strategy, we tested the effect of scavenging Aβ peptides prior to Aβ plaque formation. We demonstrate that an Aβ binding anticalin protein (Aβ-anticalin) can suppress early neuronal hyperactivity. Unexpectedly, the sole targeting of Aβ monomers was sufficient for the hyperactivity-suppressing effect of the Aβ-anticalin. Biochemical and neurophysiological analysis suggest that Aβ-anticalin-dependent depletion of naturally secreted Aβ monomers interrupts aggregation to neurotoxic oligomers and, thereby, prevents synaptic dysfunction. Our results demonstrate that Aβ monomer scavenging can reverse early neuronal dysfunction and, thus, offers a promising strategy for the preventive treatment of AD.

Introduction

How to halt Alzheimer's disease (AD) and the associated cognitive decline and memory loss remains one of the major challenges in the research of brain diseases. According to the amyloid-β (Aβ) hypothesis, Aβ peptides and, especially, their soluble aggregates comprising dimers and small Aβ oligomers are the most toxic agents that perturb the integrity of neuronal structure and function [1]. Aβ peptides were also shown to cause inflammation [2], tau hyperphosphorylation [3] and, ultimately, cell death [4]. In view of these observations, the depletion of Aβ is expected to slow down or, hopefully, even prevent the cognitive decline associated with Alzheimer's disease in affected individuals.

Treatment strategies aiming at the scavenging of Aβ by passive immunization with antibodies have largely failed to show a significant deceleration of cognitive decline in clinical studies, in fact raising concerns about the amyloid hypothesis [5]. Similar discouraging observations were made in Alzheimer's mouse models [6,7].There are several possible explanations for the general failure of these approaches, most prominently an inadequate timing of the therapeutic intervention, after the brain has already undergone irreparable damage [8].

Only recently, groundbreaking results were reported for the monoclonal antibodies (mAb), foremost Lecanemab, which preferentially binds protofibrils (> 75 kDa soluble Aβ aggregates) and significantly reduced cognitive decline in patients with early AD in a phase 3 study [9]. Moreover, anti-Aβ treatment at very early stages of development had positive outcomes in mouse models of β-amyloidosis. Thus, it has been demonstrated that, before Aβ plaque formation, the prevention of extracellular Aβ accumulation involving the use of γ-secretase inhibitors can effectively abolish neuronal hyperactivity [10]. This is relevant because a variety of studies in mice and humans have established that neuronal hyperactivity is probably the earliest form of neuronal dysfunction in the diseased brain [10–17]. This neuronal hyperactivity can be induced directly by the accumulation of soluble Aβ dimers, the smallest of all oligomers. It develops prior to Aβ plaque formation [10] and is mechanistically linked to aberrant synaptic glutamatergic transmission [18].

In view of the ineffectiveness of Aβ-scavenging antibodies to reverse neuronal dysfunctions in previous mouse studies [6], we applied here an alternative Aβ-scavenging strategy based on the anticalin technology [19]. Anticalins are proteins that are selected via phage display from a random library based on the human lipocalin protein scaffold and further engineered for optimal pharmacological properties. Anticalins exhibit very high target affinities and low immunogenic potential [20]. These properties make them an alternative therapeutic entity to antibodies, particularly if immunological effector functions are not desired, such as in the case of many neurological disorders. Anticalins have already entered clinical trials for different indications [21]. Several Aβ-binding anticalins with high affinities and specificities for the monomeric peptide target have recently been described [22], and their mode of tight complex formation with the central Aβ epitope (Lys^{P16} to Lys^{P28}) – which is common to both $Aβ_{40}$ and $Aβ_{42}$ peptide species – was elucidated by X-ray crystallography [23].

Results

Aβ-anticalins prevent neuronal dysfunction

We produced the anticalin H1GA (dubbed Aβ-anticalin) **(**Fig. 1A**)** in Escherichia coli and purified it to homogeneity as previously described **(Fig. S1**, materials and methods). The recombinant protein was biochemically characterized by ESI mass spectrometry and confirmation of binding activity towards the monomeric Aβ(1–40) peptide using real-time surface plasmon resonance (SPR) spectroscopy. In our experimental setup, this Aβ-anticalin solution was directly applied *in vivo* to the exposed hippocampal CA1 region [10,18] of 2-3-month-old APP23xPS45 mice, at a stage preceding the formation of Aβ plaques [14]. In this way, problems of brain delivery, involving systemic application of this protein, were circumvented. Simultaneously, we monitored changes in neuronal activity at single-cell resolution by using two-photon calcium imaging (Fig. 1B, C).

In line with previous observations made for the same animal model under similar conditions [10], we registered a marked hyperactivity in a fraction of neurons under baseline conditions (Fig. 1D left). Local application of Aβ-anticalin to the monitored CA1 neurons rapidly suppressed the hyperactivity (Fig. 1D middle, S2A). Notably, the Aβ-anticalin effect was largely reversible after a washout period of only 5–10 min (Fig. 1D right, **S2B**).

We have previously established that, at these early stages, neuronal dysfunction of hippocampal CA1 pyramidal neurons in mouse models of β-amyloidosis is characterized mainly by the emergence of hyperactive neurons [10]. Aβ-anticalin treatment reduced the number of hyperactive cells in APP23xPS45 mice to the same levels observed in wild type mice (Fig. 1E). Moreover, a cell-by-cell analysis revealed that Aβ-anticalin treatment reduced neuronal activity levels across the entire frequency range and, in treated mice, the neuronal activity distribution was undiscernible from that of wild type mice **(**Fig. 1F, **Fig. S2 C-E**).

Control experiments demonstrated that the application of the Aβ-anticalin did not alter activity levels in wild type mice (**Fig. S3 A, B**). Likewise, the application of the recombinant human lipocalin 2, the protein from which the anticalin originates and which does not bind Aβ in vitro [22], was ineffective in APP23xPS45 mice as it did not reduce the number of hyperactive neurons (**Fig. S3 C, D**). Collectively, these results establish that the hyperactivity-reducing effect of Aβ-anticalins depends critically on the interaction with APP transgene expression and suggest that Aβ-anticalins have no activity-changing side effects in wild type animals.

Next, as an independent test for the anti-Aβ action of the Aβ-anticalin, we explored its effects on neuronal hyperactivity, which was experimentally induced through the direct application of Aβ to the hippocampus of wild type mice [10,18]. For this experiment, we used the synthetic disulfide cross-linked Aβ dimer $[AβS26C]_2$, which was shown to be a potent neurotoxic Aβ-agent in various assays, including neurite outgrowth [3], the induction of long-term potentiation (LTP) [24,25] and neuronal hyperactivation [10,18]. It is important to note that in all these assays, applications of $[AβS26C]_2$ faithfully reproduced the actions of human Aβ extracts and, in particular, those of natural Aβ dimers.

In line with earlier reports [10,18], we first observed that the local application of $[AβS26C]_2$ to hippocampal CA1 neurons caused a robust neuronal hyperactivation (Fig. 2A, B). However, in contrast to the hyperactivity-blocking effect in the transgenic mice, the Aβ-anticalin did not have any blocking action on the $[AβS26C]_2$–induced hyperactivity in wild type mice (Fig. 2C, D) and the actions of both applications were undiscernible (Fig. 2, E-G). While this result may be expected based on the binding properties of the Aβ-anticalin [23], it is still remarkable as $[AβS26C]_2$ mimics the action of human Aβ dimers [18]. Thus, the experiment does not answer whether binding to monomers or dimers is necessary for the hyperactivity-reducing action of the Aβ-anticalin but warrants further investigation of the interaction of the anticalin with different forms of Aβ.

We have previously demonstrated that the Aβ-anticalin binds Aβ monomers with high affinity [22,23]. To determine the precise Aβ-binding behavior of the Aβ-anticalin, we performed size exclusion chromatography (SEC) of the Aβ-anticalin alone, and after mixture with freshly prepared Aβ monomers. Compared to the isolated Aβ-anticalin (Fig. 3A, B), we observed a shift of the elution volume after combination with freshly prepared Aβ monomers, corresponding to an increase in size by approximately 4.4 kDa (Fig. 3C), in line with the known mass of 4430 Da for the Aβ monomer.

In light of the strong affinity for monomers, we asked whether binding Aβ monomers by the Aβ-anticalin directly prevented their neurotoxic actions. In agreement with previous reports that Aβ monomers do not impair LTP [26] or neurite outgrowth [27] as well as the observation that human brain-derived monomers do not cause neuronal hyperactivation [18], we observed that the administration of a freshly prepared synthetic Aβ monomer solution *in vivo* did not cause neuronal hyperactivation in CA1 in wild type mice (Fig. 3D, E**)**. To exclude a dose-dependent effect, we also performed two-photon imaging in acutely prepared hippocampal slices, in which neuronal *in vivo*-like baseline activity had been induced by the

application of bicuculline (**Fig. S4**). Under these conditions, the application of 1 µM or 100 µM solutions of the Aβ monomers did not produce neuronal hyperactivation (Fig. 3F, G).

The Aβ-anticalin prevents Aβ oligomerization

As Aβ monomers, themselves, did not induce neuronal dysfunction, we hypothesized that scavenging of the (nascent) Aβ monomers by the Aβ-anticalin must reduce the concentration of toxic Aβ oligomers in the brain, either by preventing their formation or by facilitating their disintegration.

To surveil the aggregation behavior of Aβ, we used a Thioflavin T (ThT) fluorescence assay as a probe for the formation of β-sheets [28] that are characteristic for Aβ fibrils. We performed an Aβ 'aging' experiment, in which incubated Aβ monomers immediately started forming β-sheet aggregates as demonstrated by a steep initial increase in the ThT-fluorescence, which decayed after approximately two hours indicating completion of aggregate/fibril formation (Fig. 4A) [29]. The addition of the Aβ-anticalin at the beginning of the incubation period, however, fully prevented the formation of ThT-positive Aβ fibrils (Fig. 4B) as previously demonstrated by transmission electron microscopy [22]. In contrast, the addition of the Aβ-anticalin after 90 minutes, i.e. after ThT-positive fibrils had formed, did not reduce fluorescence, indicating that preformed fibrils were not dissolved by the addition of the Aβ-anticalin (Fig. 4C).

Based on the kinetics of Aβ aggregate/fibril formation, we conclude that the freshly prepared synthetic Aβ monomers immediately start forming aggregates and assume that Aβ oligomers should arise as an intermediate step on the way to final fibril formation [30]. To test this, we applied the 'aged' Aβ solution, i.e. Aβ, which had been incubated for 90–120 minutes (Fig. 4D), to CA1 pyramidal neurons of wild type mice *in vivo*, which robustly induced neuronal hyperactivation (Fig. 4E, J), in contrast to the observed ineffectiveness of the freshly prepared monomer solution (Fig. 3). Likewise, 'aged' Aβ application also caused neuronal hyperactivation in hippocampal slices, both at concentrations of 1 and 100 µM monomer equivalent (**Fig. S5, A to D**).

While it is clear from the ThT-fluorescence assay that the Aβ-anticalin prevents the formation of Aβ fibrils (Fig. 4B), we asked whether the Aβ-anticalin could also prevent the formation of toxic soluble Aβ dimers and oligomers. Thus, we next administered the solution of Aβ monomers, which had been incubated *in vitro* with a stoichiometric concentration (1:1) of the Aβ-anticalin for 90–120 minutes (Fig. 4F). The application of this solution *in vivo* did not induce neuronal hyperactivation (Fig. 4G, K), demonstrating, first, that toxic Aβ dimers or oligomers had not formed and, second, that anticalin-bound Aβ monomers do not induce neuronal hyperactivation (Fig. 4L). Likewise, the application of this solution did not change the neuronal activity levels in bicuculline-treated hippocampal slices (**Fig. S5, E and F**).

Finally, we asked whether the neutralizing effect of the Aβ-anticalin might at least partially be mediated by the disintegration of neurotoxic Aβ aggregates. When we applied the mixture of 'aged' Aβ and Aβ-anticalin (Fig. 4C) in the hippocampal CA1 region *in vivo*, it induced neuronal hyperactivation (Fig. 4I, M) which was undiscernible from that caused by the Aβ oligomers alone (Fig. 4N**)**. In line with this, in the SEC, we found a slight shift to lower elution volume (in line with larger size by ~ 2.7 kDa) as well as a

broadening of the peak corresponding to the Aβ-anticalin compared to the anticalin protein alone (**Fig. S6**). This indicates binding of Aβ monomers but not larger oligomers or aggregates to the Aβ-anticalin. Therefore, we conclude that application of the Aβ-anticalin is ineffective in preventing Aβ-dependent neuronal hyperactivation once toxic Aβ aggregates have formed.

Prevention of excessive glutamate accumulation by Aβ-anticalin

At the synaptic level, Aβ-dependent neuronal hyperactivity is associated with the accumulation of extracellular glutamate [18,31–33]. To investigate whether the Aβ-anticalin prevents this synaptic impairment, we performed two-photon imaging of synaptically released glutamate in hippocampal slices. To this end, we virally expressed the fluorescent glutamate sensor SF-iGluSnFR A184S [34] unilaterally in the hippocampal CA1 region of wild type mice *in vivo* (Fig. 5A). After 2–3 weeks of viral expression, we performed two-photon population imaging of synaptically evoked glutamate transients in the stratum radiatum of CA1 (Fig. 5B) by electric stimulation of the Schaffer collaterals [35] (Fig. 5C left). The application of 'aged' Aβ-solution (Fig. 4A) caused a robust increase in the synaptically evoked glutamate transients (Fig. 5C middle), which was reversible after a washout of 5–10 minutes (Fig. 5C right). These results were similar to previous results with $[AβS26C]_2$ [18]. In contrast, the application of a similarly 'aged' solution of an Aβ(40 – 1) peptide with reverse sequence, which does not form aggregates [36], did not affect synaptically evoked glutamate transients (Fig. 5D). In a parallel approach, injection of solution incubated with Aβ-anticalin (Fig. 4B), putatively containing bound Aβ monomers, did not enhance synaptically evoked glutamate transients (Fig. 5E, F). Likewise, the application of the Aβ-anticalin alone did not affect the evoked glutamate transients (**Fig. S7**). Together, this data demonstrates that preventing the formation of toxic Aβ oligomers or aggregates also prevented the synaptic dysfunction underlying Aβ-induced neuronal hyperactivity.

Discussion

In this study, we demonstrate that scavenging Aβ monomers can restore normal neuronal activity levels in mouse models of AD and provide mechanistic evidence for the rescue action of the Aβ-anticalin. Under disease conditions, naturally secreted Aβ monomers, which are pathologically inactive, rapidly form toxic dimers and oligomers which cause neuronal hyperactivity in vivo. However, adding the Aβ-anticalin at the beginning of the aggregation cascade scavenges Aβ monomers, thereby preventing the formation of toxic aggregates. In consequence, neuronal activity levels remain unaltered (Fig. 5G).

Hippocampal hyperactivity is an early neuronal dysfunction of AD in mice and humans, precedes plaque deposition as well as overt brain atrophy [17,37] and is associated with the break-down of circuits and impaired cognition [38–40]. Moreover, studies in mice and humans demonstrated that the effective suppression of neuronal hyperactivity can improve or even restore cognitive function [41,42]. Neuronal hyperactivity can be prevented reduced in mouse models by blocking Aβ secretion [10,42], but previous

attempts at scavenging Aβ using mAbs have even exacerbated neuronal dysfunction [6]. In consequence, our findings that Aβ-anticalin treatment can restore normal neuronal activity demonstrate the feasibility of such approaches. Moreover, we provide evidence that scavenging of Aβ prevented glutamate accumulation, a prominent feature of AD, which is associated with impaired synaptic integrity and plasticity as well as the underpinning of neuronal hyperactivity [18,31].

In line with previous reports [18,26,27], we found that Aβ monomers are pathologically inert. Thus, solutions containing the Aβ monomers only or Aβ monomers stably bound by the Aβ-anticalin failed to induce neuronal hyperactivity both *in vivo* and *in vitro* and, furthermore, did not lead to extracellular glutamate accumulation. On the contrary, a solution of aggregated, i.e. 'aged', Aβ including dimers and oligomers, potently perturbed neuronal function. These observations reinforce previous findings that such oligomers are the most toxic species of Aβ [18,24,43,44].

In light of this, the rapidity of the hyperactivity-reducing effect of the Aβ-anticalin application *in vivo* is remarkable because the brains of APP23xPS45 mice already contain elevated levels of oligomeric Aβ [42]. Thus, our data suggest that neuronal dysfunction in early AD largely depends on the continuous de novo release of (nascent) Aβ monomers, which immediately start forming toxic oligomers or aggregates rather than a stable pool of such Aβ species. This notion is in line with earlier reports that γ-secretase-inhibition, which prevents the release of the Aβ peptide into the extracellular space [45], leads to a rapid decrease of total [46,47] and oligomeric [10] Aβ levels in mouse models of β-amyloidosis and, concomitantly, normalized neuronal activity [10]. In consequence, it is likely that existing oligomers are quickly rendered innocuous *in vivo*, either by clearance from the brain or by to the formation of larger, less toxic aggregates [44]. While previous findings did not exclude that oligomers can form intracellularly before they are released [48–50], based on the effectivity of the Aβ-anticalin in APP23xPS45 mice, it is unlikely that released oligomers reach sufficiently high concentrations to cause neuronal dysfunction *in vivo*. Thus, taken together, our data indicate that an Aβ-anticalin can prevent Aβ-induced neurotoxic effects by scavenging the monomeric peptide and interfering with its aggregation without the need or ability of the Aβ-anticalin to dissolve preexisting oligomers.

Anticalins exhibit several beneficial properties compared with mAbs, in particular small size, high specificity and strong affinity for Aβ [22], including a lack of interaction with plasma proteins [23], as well as low immunogenic potential [20]. This may be in contrast to the use with the humanized IgG1 Lecanemab that caused clear side effects in a significant fraction of treated Alzheimer patients, including microhemorrhages and macrohemorrhages [9]. Thus, Aβ-anticalins appear as promising candidates for preventive amyloid-scavenging strategies in longitudinal studies, potentially leading to their development as novel therapeutic entities for clinical application.

Methods

Animal models

All experimental procedures were performed in compliance with institutional animal welfare guidelines and were explicitly approved by the local governments. *In vivo* experiments were performed with 8–12 week-old C57 Bl/6N wild type mice of both sexes or with age-matched female APP23xPS45 mice expressing the APP Swedish mutation (670/671) and the G384A mutation in the presenilin 1 (PS1) gene under the Thy-1 promotor [14]. All mice were housed in standard mouse cages under a 12-h dark/12-h light cycle and constant temperature and humidity. Food and water was provided *ad libitum*.

Surgery

In vivo two-photon imaging was performed as described previously [10,18]. In brief, mice were initially anesthetized with isoflurane (2% vol/vol in pure O_2). The scalp was partially removed and a custom-made plastic recording chamber with a central opening was attached to the skull using dental cement. The skull was thinned with a dental drill (Meisinger, Neuss, Germany) in a circle with a diameter of approximately 2 mm with the center on top of the hippocampal CA1 region (AP -2.75, ML 3.5) and the recording chamber was filled with artificial cerebrospinal fluid (ACSF; 125 mM NaCl, 4.5 mM KCl, 26 mM $NaHCO_3$, 1.25 mM NaH_2PO_4, 2 mM $CaCl_2$, 1 mM $MgCl_2$, 20 mM glucose, pH 7.4 when bubbled with carbogen gas), which had been warmed to 37°C. The bone was carefully removed with a thin cannula to open a cranial window directly above the imaged region. The dura and cortical tissue covering the hippocampus were removed by suction. After this, multi-cell bolus loading was performed with the organic Ca^{2+}-indicator Cal-520 AM [51], injected through a glass patch pipette 200 µm underneath the hippocampal surface. After the surgery was completed, the concentration of Isoflurane was reduced to 0.8-1.0% vol/vol for imaging.

Anticalin preparation

The Aβ-specific Anticalin was prepared via soluble cytoplasmic expression in 2 L shake flask cultures of *E. coli* Origami B [52]. Wild type Lcn2 was periplasmatically expressed in *E. coli* W3310 [53,54]. Both proteins were purified by His_6-tag affinity chromatography [55] and SEC on a Superdex 75 HR 26/60 column (GE Healthcare, Munich, Germany) using HEPES-Ringer (135 mM NaCl, 5 mM KCl, 2 mM $CaCl_2$, 1 mM $MgCl_2$, 10 mM HEPES, 20 mM Glucose, pH 4.7) or phosphate-buffered saline (PBS; 4 mM KH2PO4, 16 mM Na2HPO4, 115 mM NaCl, pH 7.4). Protein purity was checked by SDS/PAGE [56] and ESI mass spectrometry on an maXis instrument (Bruker Daltronics, Bremen, Germany) in the positive ion mode. Endotoxins were removed using NoEndo™ HC (High Capacity) Spin Columns (Protein Ark, Rotherham, UK) and residual pyrogen levels were analyzed using the Endosafe-PTS™ (Charles River Laboratories International, Inc., Wilmington, MA, USA) resulting in < 5 EU/mL. Protein concentration was determined via absorption at 280 nm using molar absorption coefficients calculated with the ExPASy ProtParam tool [57]. Proteins were stored at -20°C. Immediately before the experiment, the anticalin was diluted in ACSF or HEPES-ringer.

Aβ peptides

Aβ(1–40) and Aβ(40 – 1), with a reverse amino acid sequence, were obtained from Bachem Pharmaceuticals (Bubendorf, Germany). The Aβ(1–40/S26C) dimer $[AβS26C]_2$ was from jpt (Berlin,

Germany). All peptides were dissolved in DMSO and stored frozen. Immediately before the experiments, the peptides were thawed and diluted in ACSF or HEPES-Ringer or in Ringer solution containing an equimolar amount of the Aβ-anticalin. The solution was pressure-applied through a glass patch pipette either immediately or incubated at room temperature (25°C) for the indicated time, centrifuged at 6000 rpm for 5 minutes to remove insoluble aggregates before application.

Hippocampal slice preparation

Mice were anesthetized and decapitated. The brain was surgically removed and submerged in ice-cold slicing solution (24.7 mM glucose, 2.48 mM KCl, 65.47 mM NaCl, 25.98 mM $NaHCO_3$, 105 mM sucrose, 0.5 mM $CaCl_2$, 7 mM $MgCl_2$, 1.25 mM NaH_2PO_4, 1.7 mM ascorbic acid) with an osmolarity of 290–300 mOsm and a pH of 7.4, which was stabilized by bubbling with carbogen gas. Horizontal slices (300 µm) were cut using a vibratome. These were allowed to recover at room temperature for at least one hour in a recovery solution containing 2 mM $CaCl_2$, 12.5 mM glucose, 2.5 mM KCl, 2 mM $MgCl_2$, 119 mM NaCl, 26 mM $NaHCO_3$, 1.25 mM NaH_2PO_4, 2 mM thiourea (Sigma, St. Louis, USA), 5 mM Na-ascorbate (Sigma), 3 mM Na-pyruvate (Sigma), and 1 mM glutathione monoethyl ester. The pH was adjusted to 7.4 with HCl, and the osmolarity was 290 mOsm. Before the imaging experiment, the Schaffer collaterals were cut and the slices were transferred into the recording setup and superfused with warmed (37°C) ACSF. To induce *in vivo*-like ongoing baseline activity in the hippocampal slices, 100 µM bicuculline was added to the ACSF and the potassium concentration was slowly increased to 5.5–6.5 mM (for a detailed description, see [18]). For calcium imaging experiments, bolus loading of Cal-520 AM was performed as described above.

Two-photon Ca^{2+}-imaging and application of Aβ and/or anticalins

In vivo and *in vitro* two-photon Ca^{2+} imaging was performed in the same custom-made multi-photon recording setup based on an upright microscope (Olympus, Shinjuku, Japan) as described previously [18]. Excitation light was provided by a tunable Ti:sapphire laser at a wavelength of 920 nm (Coherent, Santa Clara, USA). Fluorescence images were collected using a resonant galvo mirror scanner operating at 8 or 12 kHz (GSI group, Bedford, USA) as well as a 40x 0.8 NA objective (Nikon, Tokyo, Japan). Full frames were acquired at 40 Hz.

After surgery or slice preparation and Cal-520 AM bolus loading (see above), spontaneous Ca^{2+} -transients were recorded from the pyramidal layer of hippocampal CA1. For the injection of Aβ and/or anticalins a glass patch pipette (tip resistance 1–2 MΩ) was filled with approximately 5 µl of the peptide/protein application solution (see above) and the tip was positioned in the pyramidal layer of the hippocampal CA1 region under visual control (about 150 µm under the hippocampal surface *in vivo* or 50 µm below the slice surface *in vitro*). Pressure was carefully applied using a picospritzer II (Parker, Cleveland, USA) until a slight tissue displacement in front of the tip indicated fluid ejection (typically around 20 mBar). In some experiments, this was further validated by adding 5 µM Alexa 594 dye (Thermo

Fischer, Waltham, USA) to the pipette solution. The pressure was stopped after 30–60 seconds. The same cells were monitored during baseline, pressure application and washout conditions.

Virus injection and SF-iGluSnFR imaging

AAV2/1.hSynapsin.iGluSnFR A184S (*44*) was a gift from Loren Looger (HHMI/Janelia). Virus injection and two-photon population glutamate imaging was performed as described previously [18,35]. In brief, 500nl of AAV2/1.hSynapsin.iGluSnFR A184S ($2.4x10^{12}$ gc/ml) were injected into the hippocampal CA1 region (AP -2.75, ML 3.5 and DV 2–3 mm) of isoflurane-anesthetized 4–6 week-old wild type mice by slow (of 10–20 nl/min) pressure injection from a glass pipette. After the retraction of the injection pipette, mice were transferred back to their home cage, where 2–3 weeks were allowed for viral expression.

After that, hippocampal slices were prepared as described further above and glutamate two-photon imaging of synaptically evoked (electrical stimulation of the Schaffer collaterals, 100 µsec, 30-40V) glutamate transients was performed in the stratum radiatum of the hippocampal CA1 area under illumination at 920 nm with a framerate of 120 Hz. Aβ peptide and/or anticalin were pressure applied in the field of view through a second glass pipette.

Image analysis

Offline image analysis was performed as described previously [58]. Fluorescence traces were extracted from the imaging data using custom-written software based on LabVIEW. In Ca^{2+}-imaging experiments, neurons were visually identified and regions of interest (ROIs) were drawn around their somata. Astrocytes were excluded from the analysis due to their morphology and their high fluorescence levels [59]. In glutamate imaging, a region of interest (ROI) was drawn over the full imaging frame. The fluorescence of each ROI over time was extracted, low-pass filtered to 10 Hz (Ca^{2+}) or 40 Hz (glutamate) and normalized to the baseline as df/f =(f(t) - f0)/f0, where f0 was set at the 10th percentile of the entire trace in Ca^{2+}-imaging or at the mean of the pre-stimulus interval in glutamate imaging experiments. Fluorescence changes with peak amplitudes three times larger than the standard deviation of the baseline were accepted as neuronal calcium or extracellular glutamate transients.

Measurement of binding activity using surface plasmon resonance (SPR)

Kinetic affinity data of the Aβ-anticalin (H1GA) and the recombinant wild type lipocalin 2 (Lcn2) were measured at 25°C on a BIAcore 2000 system (BIAcore, Uppsala, Sweden) with immobilized Aβ(1–40) (Bachem Pharmaceuticals, Bubendorf, Germany) according to a published procedure [22] using HBS-T (20 mM HEPES/NaOH pH 7.5, 150 mM NaCl and 0.005% v/v Tween20) as running buffer. ~350 RU of Aβ(1–40) was covalently immobilized on a CM5 chip (GE Healthcare) using amine coupling chemistry in 10 mM sodium acetate buffer pH 5. Dilution series of the purified lipocalin proteins were applied at a flow rate of 30 µl/min. The data were double-referenced by subtraction of the corresponding signals measured for the control channel and of the average of three buffer injections [60]. Kinetic parameters were

determined by global fitting of single-cycle kinetics with BIAevaluation software v 4.1 using the Langmuir 1:1 binding model. The equilibrium dissociation constants were calculated as $K_D = k_{off}/k_{on}$ and the statistical error was estimated as previously described [61].

Analytical size exclusion chromatography

2.5 µl of a 5 mM Aβ(1–40) monomer solution in DMSO was mixed with 247.5 µL of 50 µM Aβ-anticalin solution in HEPES-Ringer resulting in a 1:1 molar ratio of Aβ-anticalin to Aβ. In a control experiment, only the buffer without the Aβ-anticalin was used. 100 µL of the sample was cleared from aggregates by centrifugation in a bench top centrifuge (13,000 rpm, 5 min, room temperature) and directly applied to SEC. The remaining sample was incubated for 90 min at room temperature, again followed by SEC after centrifugation. The chromatography was performed on a 24 ml Superdex 75 10/300 GL column (GE Healthcare) using HEPES-Ringer buffer pH 7.4 at a flow rate of 0.5 ml/min. The column was calibrated with the following protein standards (Sigma-Aldrich, Munich, Germany): alcohol dehydrogenase (ADH, 150 kDa) bovine serum albumin (BSA, 66 kDa), ovalbumin (43 kDa), carbonic anhydrase (CA, 29 kDa), cytochrome c (Cyt c, 12.4 kDa) and aprotinin (Ap, 6.5 kDa). Blue dextran was applied to determine the void volume of the column. Based on the peak elution volumes, the partition coefficients (K_{av}) were calculated and used to interpolate the apparent molecular masses of the Aβ/anticalin mixtures.

ThioflavinT fluorescence assay

The ThT Assay was carried out according to previously published procedure [22]. Aβ(1–40) was lyophilized and dissolved in 1,1,1,3,3,3-hexafluoro-2-propanol (HFIP; Sigma Aldrich) at a concentration of 5 mg/ml. Following the evaporation of HFIP in the fume hood for 12 h, the dried Aβ(1–40) was dissolved in 250 µl ice-cold H_2O. After sonication for 15 min at 4°C (Sonorex, Bandelin, Berlin, Germany), the peptide solution was sterile-filtrated with a Costar Spin-X centrifuge tube filter, 0.45 µm pore size cellulose acetate membrane (Corning Life Sciences, Kaiserslautern, Germany). The freshly prepared solution of monomeric Aβ(1–40) was immediately used for the aggregation assay by mixing the 2mg/ml (462 µM) Aβ(1–40) monomer solution with either 250 µl Aβ-anticalin solution in PBS at a 1:1 molar ratio or PBS alone. Aggregation reactions were performed in triplicates at 25°C or 37°C in 2 ml DNA LoBind Tubes (Eppendorf, Hamburg, Germany) with stirring at 500 rpm using a 5 mm magnetic bar. For fluorescence measurements, 20 µl samples were removed at distinct time points and mixed with 180 µl of a 55.6 µM solution of Thioflavin T (ThT) (Sigma–Aldrich) in 0.5×PBS and analyzed in a FluoroMax-3 spectrofluorometer (HORIBA Jobin Yvon, Bensheim, Germany) using an excitation wavelength of 450 nm and an emission wavelength of 482 nm. The Integration time was set to 20 s with a slit width of 2 nm. Measured fluorescence intensities were set to zero for t = 0 and the asymptotic value of the fluorescence intensity of aggregated Aβ(1–40) in 0.5×PBS was set to 100%.

Statistics

For the comparison of two groups, we used two-tailed Wilcoxon signed rank or rank sum tests. For the comparison of multiple groups, we used a Kruskal-Wallis test with Dunn-Sidac post-hoc comparison or a

Kolmogorov-Smirnov-Test. Details on the exact statistical test used as well as the number of subjects and samples are included in the respective figure legends. Results are displayed as mean ± SEM.

Declarations

Acknowledgments

We thank C. Karrer, F. Beyer, S. Achatz and G. Finck for technical support. We are grateful to L. Looger for providing SF-iGluSnFR constructs. This work was funded by the German Research Foundation (DFG grant no. 685472) to BZ and the Max Planck School of Cognition. BZ is a is an Albrecht-Struppler-Clinician Scientist Fellow, funded by the Federal Ministry of Education and Research (BMBF) and the Free State of Bavaria under the Excellence Strategy of the Federal Government and the Länder, as well as by the Technical University of Munich - Institute for Advanced Study. AK is a Hertie-Senior-Professor for Neuroscience. MAB is supported by the UK Dementia Research Institute, which receives its funding from DRI Ltd., funded by the Medical Research Council, Alzheimer's Society and Alzheimer Research UK and by a UKRI Future Leaders Fellowship (grant number: MR/S017003/1).

Author contributions

Conceptualization and design: BZ, AS, AK; Data acquisition and interpretation: BZ, LN, CG, MMK, FU, AKD, AF, MAB; Visualization: BZ, LN, CG; Supervision: BZ, AS, AK; Writing—original draft: BZ, AK; Writing—review & editing: BZ, LN, CG, MMK, FU, AKD, AF, MAB, AS, AK

Competing interests

A.S. is founder and shareholder of Pieris Pharmaceuticals, Inc. All other authors declare no conflicts of interest. Anticalin® is a registered trademark of Pieris Pharmaceuticals GmbH, Germany.

Materials & Correspondence

Correspondence and material requests should be addressed to Benedikt Zott (benedikt.zott@tum.de).

Data availability

The authors declare that all data supporting the findings of this study areavailable within the paper and its supplementary information file. Raw data are available from the lead corresponding author upon reasonable request.

References

1. Selkoe, D. J. & Hardy, J. The amyloid hypothesis of Alzheimer's disease at 25 years. EMBO Mol Med **8**, 595–608, doi:10.15252/emmm.201606210 (2016).

2. Hong, S. *et al.* Complement and microglia mediate early synapse loss in Alzheimer mouse models. Science **352**, 712–716, doi:10.1126/science.aad8373 (2016).
3. Jin, M. *et al.* Soluble amyloid beta-protein dimers isolated from Alzheimer cortex directly induce Tau hyperphosphorylation and neuritic degeneration. Proc Natl Acad Sci U S A **108**, 5819–5824, doi:10.1073/pnas.1017033108 (2011).
4. Kadowaki, H. *et al.* Amyloid β induces neuronal cell death through ROS-mediated ASK1 activation. Cell Death Differ **12**, 19, doi:10.1038/sj.cdd.4401528 (2004).
5. Panza, F., Lozupone, M., Logroscino, G. & Imbimbo, B. P. A critical appraisal of amyloid-beta-targeting therapies for Alzheimer disease. Nat Rev Neurol **15**, 73–88, doi:10.1038/s41582-018-0116-6 (2019).
6. Busche, M. A. *et al.* Decreased amyloid-beta and increased neuronal hyperactivity by immunotherapy in Alzheimer's models. Nat Neurosci **18**, 1725–1727, doi:10.1038/nn.4163 (2015).
7. Mably, A. J. *et al.* Anti-Abeta antibodies incapable of reducing cerebral Abeta oligomers fail to attenuate spatial reference memory deficits in J20 mice. Neurobiol Dis **82**, 372–384, doi:10.1016/j.nbd.2015.07.008 (2015).
8. Walsh, D. M. & Selkoe, D. J. Amyloid beta-protein and beyond: the path forward in Alzheimer's disease. Curr Opin Neurobiol **61**, 116–124, doi:10.1016/j.conb.2020.02.003 (2020).
9. van Dyck, C. H. *et al.* Lecanemab in Early Alzheimer's Disease. New England Journal of Medicine **388**, 9–21, doi:10.1056/NEJMoa2212948 (2022).
10. Busche, M. A. *et al.* Critical role of soluble amyloid-beta for early hippocampal hyperactivity in a mouse model of Alzheimer's disease. Proc Natl Acad Sci U S A **109**, 8740–8745, doi:10.1073/pnas.1206171109 (2012).
11. Liebscher, S., Keller, G. B., Goltstein, P. M., Bonhoeffer, T. & Hubener, M. Selective Persistence of Sensorimotor Mismatch Signals in Visual Cortex of Behaving Alzheimer's Disease Mice. Current biology: CB **26**, 956–964, doi:10.1016/j.cub.2016.01.070 (2016).
12. Zarhin, D. *et al.* Disrupted neural correlates of anesthesia and sleep reveal early circuit dysfunctions in Alzheimer models. Cell reports **38**, 110268, doi:10.1016/j.celrep.2021.110268 (2022).
13. Siskova, Z. *et al.* Dendritic structural degeneration is functionally linked to cellular hyperexcitability in a mouse model of Alzheimer's disease. Neuron **84**, 1023–1033, doi:10.1016/j.neuron.2014.10.024 (2014).
14. Busche, M. A. *et al.* Clusters of hyperactive neurons near amyloid plaques in a mouse model of Alzheimer's disease. Science **321**, 1686–1689, doi:10.1126/science.1162844 (2008).
15. Bookheimer, S. Y. *et al.* Patterns of brain activation in people at risk for Alzheimer's disease. N Engl J Med **343**, 450–456, doi:10.1056/NEJM200008173430701 (2000).
16. Dickerson, B. C. *et al.* Increased hippocampal activation in mild cognitive impairment compared to normal aging and AD. Neurology **65**, 404–411, doi:10.1212/01.wnl.0000171450.97464.49 (2005).
17. Zott, B., Busche, M. A., Sperling, R. A. & Konnerth, A. What Happens with the Circuit in Alzheimer's Disease in Mice and Humans? Annu Rev Neurosci **41**, 277–297 (2018).

18. Zott, B. *et al.* A vicious cycle of β amyloid–dependent neuronal hyperactivation. Science **365**, 559–565, doi:10.1126/science.aay0198 (2019).
19. Richter, A., Eggenstein, E. & Skerra, A. Anticalins: exploiting a non-Ig scaffold with hypervariable loops for the engineering of binding proteins. FEBS letters **588**, 213–218, doi:10.1016/j.febslet.2013.11.006 (2014).
20. Rothe, C. & Skerra, A. Anticalin® Proteins as Therapeutic Agents in Human Diseases. *BioDrugs* **32**, 233–243, doi:10.1007/s40259-018-0278-1 (2018).
21. Deuschle, F. C., Ilyukhina, E. & Skerra, A. Anticalin® proteins: from bench to bedside. *Expert opinion on biological therapy* **21**, 509–518, doi:10.1080/14712598.2021.1839046 (2021).
22. Rauth, S. *et al.* High-affinity Anticalins with aggregation-blocking activity directed against the Alzheimer beta-amyloid peptide. Biochem J **473**, 1563–1578, doi:10.1042/BCJ20160114 (2016).
23. Eichinger, A., Rauth, S., Hinz, D., Feuerbach, A. & Skerra, A. Structural basis of Alzheimer beta-amyloid peptide recognition by engineered lipocalin proteins with aggregation-blocking activity. Biological chemistry **403**, 557–571, doi:10.1515/hsz-2021-0375 (2022).
24. Shankar, G. M. *et al.* Amyloid-beta protein dimers isolated directly from Alzheimer's brains impair synaptic plasticity and memory. Nat Med **14**, 837–842, doi:10.1038/nm1782 (2008).
25. O'Nuallain, B. *et al.* Amyloid beta-protein dimers rapidly form stable synaptotoxic protofibrils. J Neurosci **30**, 14411–14419, doi:10.1523/JNEUROSCI.3537-10.2010 (2010).
26. Li, S. *et al.* Decoding the synaptic dysfunction of bioactive human AD brain soluble Abeta to inspire novel therapeutic avenues for Alzheimer's disease. Acta Neuropathol Commun **6**, 121, doi:10.1186/s40478-018-0626-x (2018).
27. Hong, W. *et al.* Diffusible, highly bioactive oligomers represent a critical minority of soluble Abeta in Alzheimer's disease brain. Acta Neuropathol **136**, 19–40, doi:10.1007/s00401-018-1846-7 (2018).
28. LeVine, H., 3rd. Quantification of beta-sheet amyloid fibril structures with thioflavin T. Methods in enzymology **309**, 274–284, doi:10.1016/s0076-6879(99)09020-5 (1999).
29. Stine, W. B., Jungbauer, L., Yu, C. & LaDu, M. J. Preparing synthetic Abeta in different aggregation states. Methods Mol Biol **670**, 13–32, doi:10.1007/978-1-60761-744-0_2 (2011).
30. Sengupta, U., Nilson, A. N. & Kayed, R. The Role of Amyloid-β Oligomers in Toxicity, Propagation, and Immunotherapy. *EBioMedicine* **6**, 42–49, doi:10.1016/j.ebiom.2016.03.035 (2016).
31. Li, S. *et al.* Soluble Abeta oligomers inhibit long-term potentiation through a mechanism involving excessive activation of extrasynaptic NR2B-containing NMDA receptors. J Neurosci **31**, 6627–6638, doi:10.1523/JNEUROSCI.0203-11.2011 (2011).
32. Zott, B. & Konnerth, A. Impairments of glutamatergic synaptic transmission in Alzheimer's disease. Seminars in Cell & Developmental Biology, doi:https://doi.org/10.1016/j.semcdb.2022.03.013 (2022).
33. Hefendehl, J. K. *et al.* Mapping synaptic glutamate transporter dysfunction in vivo to regions surrounding Abeta plaques by iGluSnFR two-photon imaging. Nat Commun **7**, 13441,

doi:10.1038/ncomms13441 (2016).

34. Marvin, J. S. *et al.* Stability, affinity, and chromatic variants of the glutamate sensor iGluSnFR. Nat Methods **15**, 936–939, doi:10.1038/s41592-018-0171-3 (2018).
35. Unger, F., Konnerth, A. & Zott, B. Population imaging of synaptically released glutamate in mouse hippocampal slices. STAR Protoc **2**, 100877, doi:10.1016/j.xpro.2021.100877 (2021).
36. Enache, T. A., Chiorcea-Paquim, A. M. & Oliveira-Brett, A. M. Amyloid-beta peptides time-dependent structural modifications: AFM and voltammetric characterization. Anal Chim Acta **926**, 36–47, doi:10.1016/j.aca.2016.04.015 (2016).
37. Sperling, R. A. *et al.* Functional alterations in memory networks in early Alzheimer's disease. Neuromolecular medicine **12**, 27–43, doi:10.1007/s12017-009-8109-7 (2010).
38. Grienberger, C. *et al.* Staged decline of neuronal function in vivo in an animal model of Alzheimer's disease. Nat Commun **3**, 774, doi:10.1038/ncomms1783 (2012).
39. Ying, J. *et al.* Disruption of the grid cell network in a mouse model of early Alzheimer's disease. Nature Communications **13**, 886, doi:10.1038/s41467-022-28551-x (2022).
40. Kunz, L. *et al.* Reduced grid-cell–like representations in adults at genetic risk for Alzheimer's disease. Science **350**, 430–433, doi:10.1126/science.aac8128 (2015).
41. Bakker, A. *et al.* Reduction of hippocampal hyperactivity improves cognition in amnestic mild cognitive impairment. Neuron **74**, 467–474, doi:10.1016/j.neuron.2012.03.023 (2012).
42. Keskin, A. D. *et al.* BACE inhibition-dependent repair of Alzheimer's pathophysiology. Proc Natl Acad Sci U S A **114**, 8631–8636, doi:10.1073/pnas.1708106114 (2017).
43. Brinkmalm, G. *et al.* Identification of neurotoxic cross-linked amyloid-beta dimers in the Alzheimer's brain. Brain **142**, 1441–1457, doi:10.1093/brain/awz066 (2019).
44. Yang, T., Li, S., Xu, H., Walsh, D. M. & Selkoe, D. J. Large Soluble Oligomers of Amyloid beta-Protein from Alzheimer Brain Are Far Less Neuroactive Than the Smaller Oligomers to Which They Dissociate. J Neurosci **37**, 152–163, doi:10.1523/JNEUROSCI.1698-16.2016 (2017).
45. Haass, C. & Steiner, H. Alzheimer disease gamma-secretase: a complex story of GxGD-type presenilin proteases. Trends Cell Biol **12**, 556–562, doi:10.1016/s0962-8924(02)02394-2 (2002).
46. Abramowski, D. *et al.* Dynamics of Abeta turnover and deposition in different beta-amyloid precursor protein transgenic mouse models following gamma-secretase inhibition. J Pharmacol Exp Ther **327**, 411–424, doi:10.1124/jpet.108.140327 (2008).
47. Dovey, H. F. *et al.* Functional gamma-secretase inhibitors reduce beta-amyloid peptide levels in brain. J Neurochem **76**, 173–181, doi:10.1046/j.1471-4159.2001.00012.x (2001).
48. Walsh, D. M., Tseng, B. P., Rydel, R. E., Podlisny, M. B. & Selkoe, D. J. The Oligomerization of Amyloid β-Protein Begins Intracellularly in Cells Derived from Human Brain. Biochemistry **39**, 10831–10839, doi:10.1021/bi001048s (2000).
49. Walsh, D. M. *et al.* Naturally secreted oligomers of amyloid beta protein potently inhibit hippocampal long-term potentiation in vivo. Nature **416**, 535–539, doi:10.1038/416535a (2002).

50. Oddo, S. *et al.* Temporal profile of amyloid-beta (Abeta) oligomerization in an in vivo model of Alzheimer disease. A link between Abeta and tau pathology. The Journal of biological chemistry **281**, 1599–1604, doi:10.1074/jbc.M507892200 (2006).
51. Stosiek, C., Garaschuk, O., Holthoff, K. & Konnerth, A. In vivo two-photon calcium imaging of neuronal networks. *Proceedings of the National Academy of Sciences* **100**, 7319–7324, doi:10.1073/pnas.1232232100 (2003).
52. Prinz, W. A., Aslund, F., Holmgren, A. & Beckwith, J. The role of the thioredoxin and glutaredoxin pathways in reducing protein disulfide bonds in the Escherichia coli cytoplasm. The Journal of biological chemistry **272**, 15661–15667, doi:10.1074/jbc.272.25.15661 (1997).
53. Studier, F. W. & Moffatt, B. A. Use of bacteriophage T7 RNA polymerase to direct selective high-level expression of cloned genes. J Mol Biol **189**, 113–130, doi:10.1016/0022-2836(86)90385-2 (1986).
54. Bachmann, B. J. Pedigrees of some mutant strains of Escherichia coli K-12. Bacteriol Rev **36**, 525–557, doi:10.1128/br.36.4.525-557.1972 (1972).
55. Skerra, A., Pfitzinger, I. & Plückthun, A. The functional expression of antibody Fv fragments in Escherichia coli: improved vectors and a generally applicable purification technique. Biotechnology (NY) **9**, 273–278, doi:10.1038/nbt0391-273 (1991).
56. Fling, S. P. & Gregerson, D. S. Peptide and protein molecular weight determination by electrophoresis using a high-molarity tris buffer system without urea. Analytical biochemistry **155**, 83–88, doi:10.1016/0003-2697(86)90228-9 (1986).
57. Gasteiger, E. *et al.* ExPASy: the proteomics server for in-depth protein knowledge and analysis. Nucleic Acids Research **31**, 3784–3788, doi:10.1093/nar/gkg563 (2003).
58. Jia, H., Rochefort, N. L., Chen, X. & Konnerth, A. In vivo two-photon imaging of sensory-evoked dendritic calcium signals in cortical neurons. Nat Protoc **6**, 28–35, doi:10.1038/nprot.2010.169 (2011).
59. Nimmerjahn, A. & Helmchen, F. In vivo labeling of cortical astrocytes with sulforhodamine 101 (SR101). *Cold Spring Harb Protoc* 2012, 326–334, doi:10.1101/pdb.prot068155 (2012).
60. Myszka, D. G. Improving biosensor analysis. J Mol Recognit **12**, 279–284, doi:10.1002/(sici)1099-1352(199909/10)12:5<279::Aid-jmr473>3.0.Co;2-3 (1999).
61. Schonfeld, D. *et al.* An engineered lipocalin specific for CTLA-4 reveals a combining site with structural and conformational features similar to antibodies. Proc Natl Acad Sci U S A **106**, 8198–8203, doi:10.1073/pnas.0813399106 (2009).

Figures

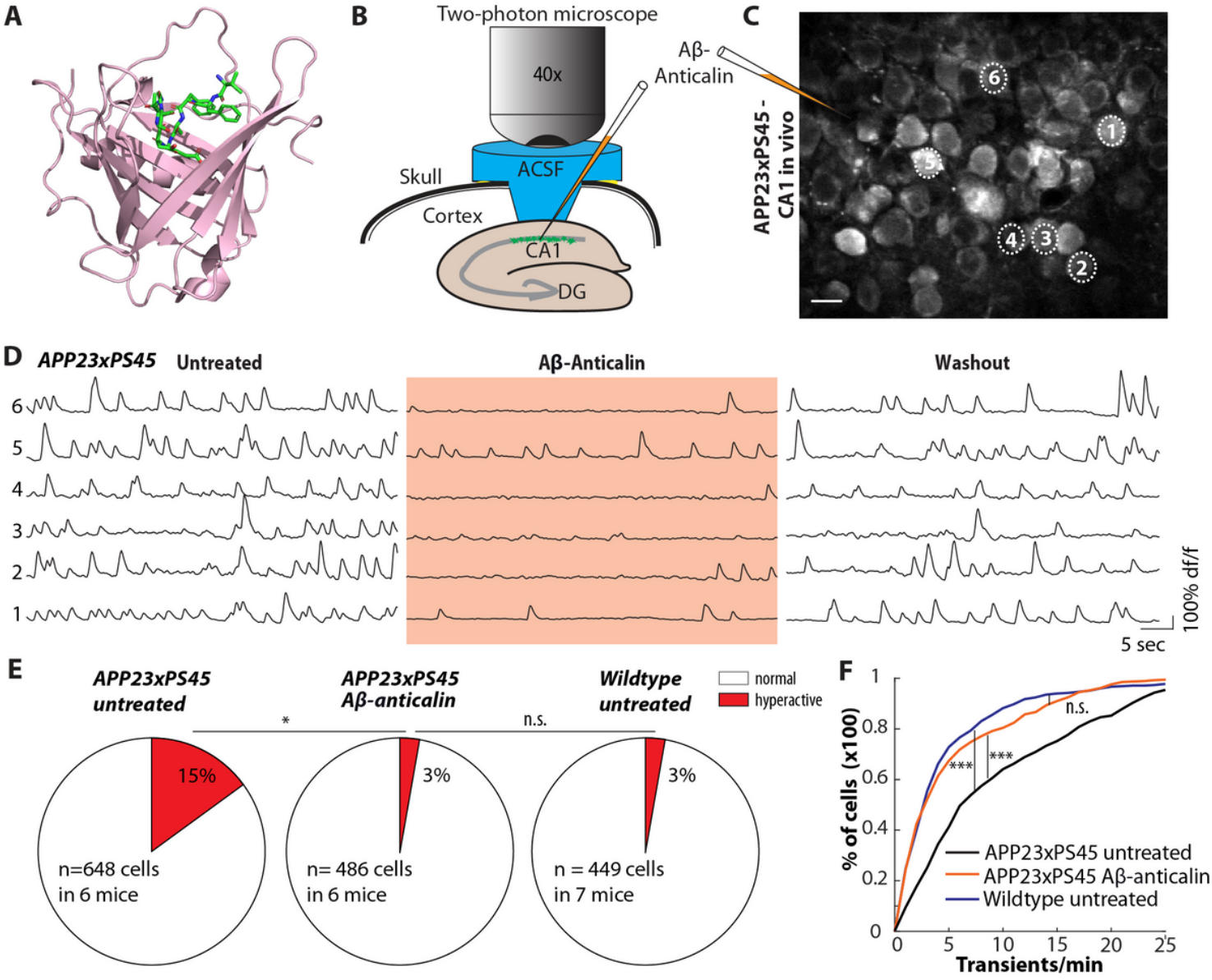

Figure 1

Aβ-anticalin treatment suppresses neuronal hyperactivity *in vivo*. (**A**) X-ray structure (PDB ID: 4MVL) of the Aβ-anticalin with its β-barrel formed by eight anti-parallel β-strands and four hypervariable loops shown in ribbon presentation. The bound central segment of the Aβ(1-40) peptide is shown as sticks and colored green. (**B**) Two-photon imaging setup for *in vivo* imaging of the hippocampal CA1 region. The filled pipette for the application of the Aβ-anticalin is indicated in orange. (**C**) Representative two-photon image of the pyramidal layer of the hippocampal CA1 region in a 2-month-old APP23xPS45 mouse after staining with the organic Ca^{2+}-indicator Cal-520 AM. The injection pipette for the application of Aβ-anticalin is visible as a dark shadow on the left side of the image and schematically outlined for clarity. (**D**) Ca^{2+}-traces recorded from the six representative neurons labeled in (C) under baseline conditions (*left*), during the application of 10 µM Aβ-anticalin (*middle*) and after a washout period of 5 min (*right*). (**E**) Percentage of hyperactive cells (more than 20 Ca^{2+}-transients per min) in untreated (*left*) and Aβ-anticalin-treated APP23xPS45 (*middle*) as well as in untreated wild type animals (right). (**F**) Cumulative

probability of the neuronal activity in untreated (black) and Aβ-anticalin-treated APP23xPS45 mice (orange) and in untreated wild type mice (blue). *p<0.05, ***p<0.001, n.s. not significant. Wilcoxon signed-rank or rank sum test (E), Kolmogorow-Smirnow-test (F).

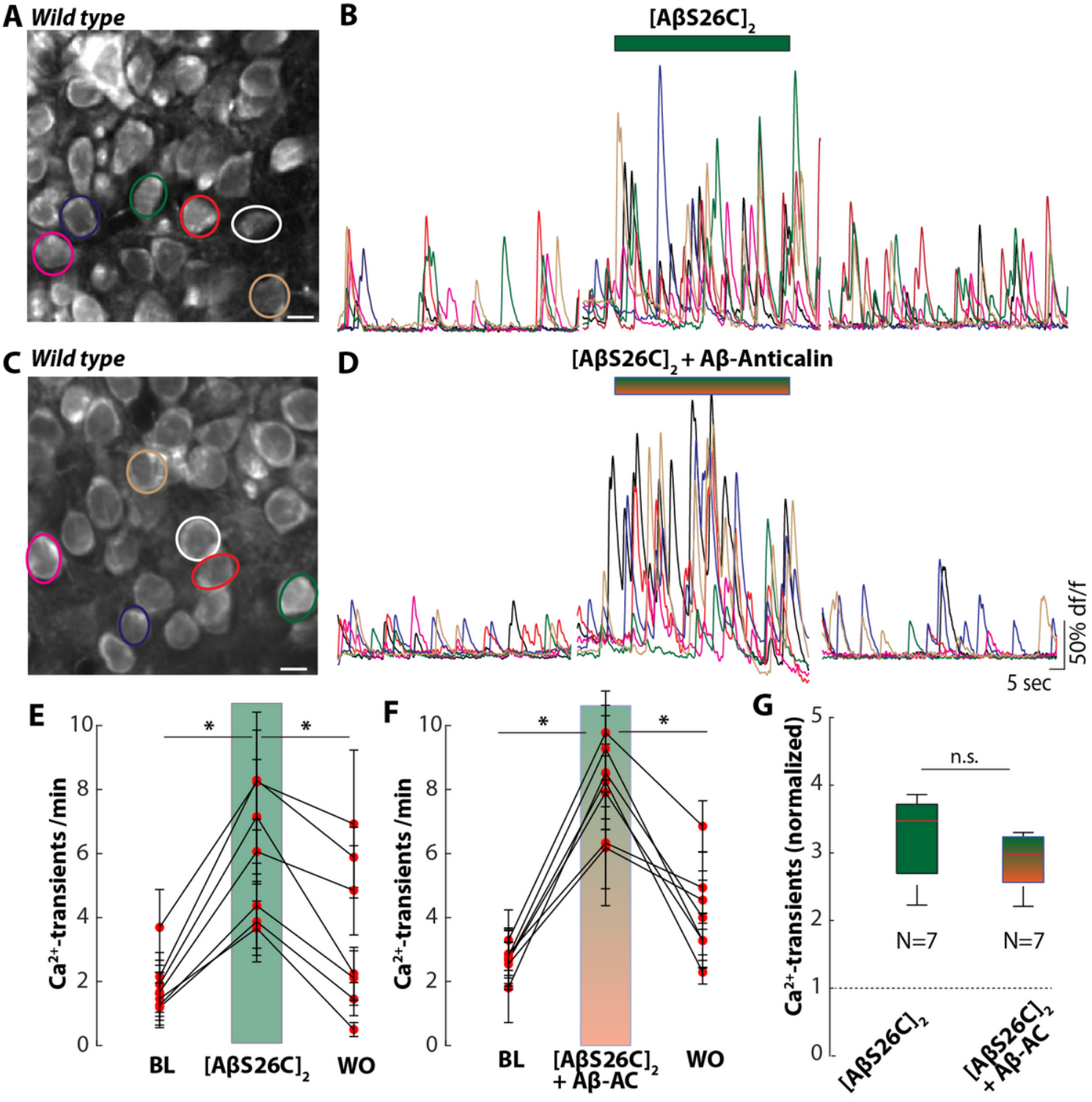

Figure 2

Ineffectivity of the Aβ-anticalin to prevent Aβ-dimer-induced neuronal hyperactivity. (A) Representative two-photon image of the pyramidal layer of the hippocampal CA1 region in a 2-month-old wild type

mouse after staining with the organic Ca^{2+}-indicator Cal-520 AM. (**B**) Superimposed representative Ca^{2+}-traces of the six neurons cycled in (A) under baseline conditions (left), during the application of 500 nM $[A\beta S26C]_2$ and after 5 min washout. The colors of the Ca^{2+}-traces correspond to the circles in (A). (**C** and **D**) same as (A and B) for the co-application of $[A\beta S26C]_2$ (500 nM) and Aβ-anticalin (1 µM). (**E**) Summary data of the application experiments in (B) from N=7 mice. Each dot represents the mean number of Ca^{2+}-transients per minute for all observed neurons in one mouse under baseline conditions (*left*), during the application of $[A\beta S26C]_2$ (*middle*), and after washout (*right*). (**F**) Same as (E) for the experiment in (D). (**G**) Number of Ca^{2+}-transients during the application of $[A\beta S26C]_2$ alone (N=7 mice) or mixed with Aβ-anticalin (N=7), normalized to the respective mean baseline activity. Scale bars: 5 µm. N.s. not significant. *p<0.05. Wilcoxon signed-rank test (E, F), Wilcoxon rank sum test (G).

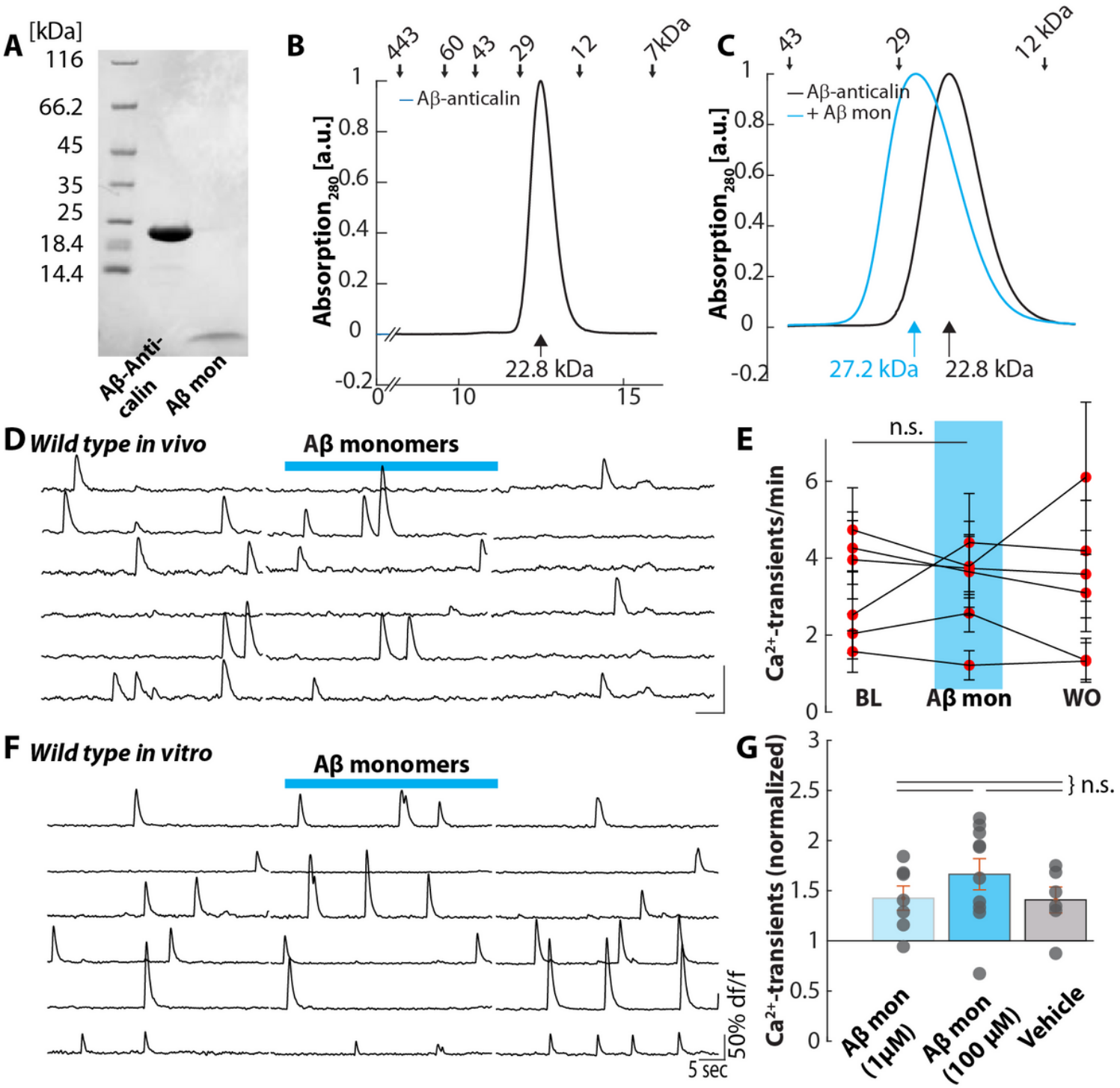

Figure 3

Aβ-anticalin binds inactive Aβ monomers. (**A**) Coomassie-stain depicting the size of Aβ-anticalin (21.3 kDa) and Aβ monomer (4.4 kDa). (**B**) Size exclusion-chromatography (SEC) of the Aβ-anticalin shows a peak at an elution volume of 12.48 ml, corresponding to an apparent molar weight of 22.7 kDa. (**C**) SEC of freshly prepared Aβ(1-40) monomers (calculated molar weight: 4430 Da) in combination with Aβ-anticalin demonstrate a shift of the peak from 12.48 to 12.07 ml, suggesting binding of the 4.4 kDa-peptide by the anticalin. (**D**) Representative Ca^{2+}-traces recorded from six hippocampal CA1 neurons of a wild type mouse under baseline conditions, during the application of Aβ monomers (10 μM, applied 5 min

after preparation of the solution) and after a washout period of 5 min. (**E**) Summary data of the experiments in (D) from N=6 mice. Each dot represents the mean number of Ca^{2+}- transients per minute, for all observed neurons in one mouse under baseline conditions, during the application of Aβ monomers and under washout conditions. (**F**) Ca^{2+}-transients from six representative CA1 pyramidal neurons in a bicuculline-treated hippocampal slice from a wild type mouse under baseline conditions (*left*), during the application of Aβ(1-40) monomers (1 µM, applied 5 minutes after preparation of the aqueous solution) through a patch pipette (*middle*) and after washout for five minutes (*right*). (**G**) Number of Ca^{2+}-transients during the application of 1 µM Aβ monomers (N=6 slices), 100 µM Aβ monomers (N=9) or ACSF as vehicle solution (N=6), normalized to the respective mean baseline activity. n.s. not significant. Error bars depict SEM. Wilcoxon signed rank test (E) or Kruskal-Wallis test with Dunn-Sidac post-hoc comparison (G).

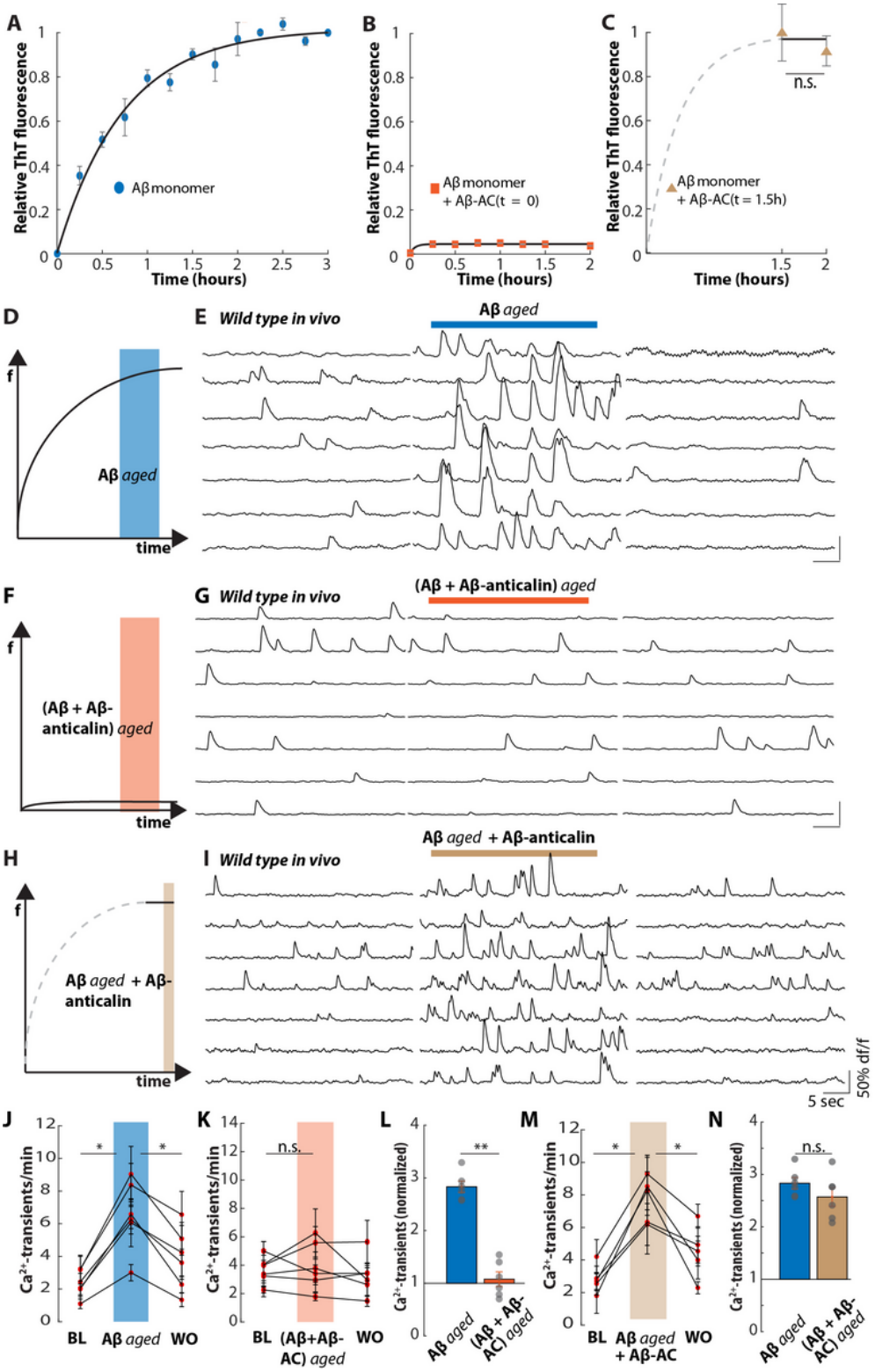

Figure 4

Prevention of the formation of toxic aggregates of the Aβ-anticalin. (**A**) *In vitro* aggregation assay of synthetic Aβ(1-40) monomers. Aβ monomers (231 μM) were incubated at room temperature and samples were taken periodically, mixed with ThT (1:10) and analyzed for fluorescence. Average (n= 3 experiments) and SEM are shown. The values were normalized to the maximum fluorescence detected. (**B**) same as (A) for samples taken from the Aβ aggregation assay in the presence of the Aβ-anticalin. (**C**) Aβ monomers

were incubated at room temperature. After 90 minutes, a sample was mixed with ThT and analyzed for fluorescence (the dotted line indicates the assumed aggregation curve based on the measurements in A). Immediately after the sample was taken, the Aβ-anticalin was added and the solution was incubated for another 30 minutes, when a second sample was analyzed. The fluorescence values were normalized to the value at t=90 (n=6). (**D**) Scheme depicting the aggregation curve of Aβ(1-40) monomers in the ThT assay. After 90-120 min, the solution should contain predominantly oligomers or aggregates (*blue zone*). (**E**) Representative Ca^{2+}-traces recorded from seven hippocampal CA1 neurons of a wild type mouse under baseline conditions, during the application of putative Aβ oligomers (10 µM monomer equivalent, applied after 90-120 min of incubation in ACSF and centrifugation) and after a washout period of 5 min. (**F**) Scheme depicting the ThT aggregation assay in the presence of the Aβ-anticalin (10 µM Aβ(1-40) monomers, 10 µM Aβ-anticalin). After 90-120 min incubation (orange zone), the solution should predominantly contain protein-bound Aβ monomers. (**G**) Same as (E) for the application of putative protein-bound Aβ monomers. (**H**) Scheme depicting the aggregation of Aβ monomers alone for 90 minutes and in presence of the Aβ-anticalin for the same period. (**I**) Same as (E) for the application of 'aged' Aβ (10 µM monomer equivalent), which had been incubated with 10 µM Aβ-anticalin for further 30 min. (**J**) Summary data of the experiments in (E) from N=6 mice. Each dot represents the mean number of Ca^{2+}- transients per minute, for all observed neurons in one mouse under baseline conditions, during the application of 'aged' Aβ and under washout conditions. (**K**) same as (J) for the experiment in (G) and the application of Aβ/Aβ-anticalin. (**L**) Number of Ca^{2+}-transients during the application of 'aged' Aβ (N=6) or Aβ/Aβ-anticalin (N=6), normalized to the respective mean baseline activity. (**M**) same as (J) for the experiment in (I) and the application of 'aged' Aβ, incubated with Aβ-anticalin. (**N**) Number of Ca^{2+}-transients during the application of 'aged' Aβ (N=6) or 'aged' Aβ, incubated with Aβ-anticalin (N=6), normalized to the respective mean baseline activity. n.s. not significant, *p<0.05, **p<0.005, Wilcoxon signed-rank test (J, K, M), Wilcoxon rank sum test (C, L, N).

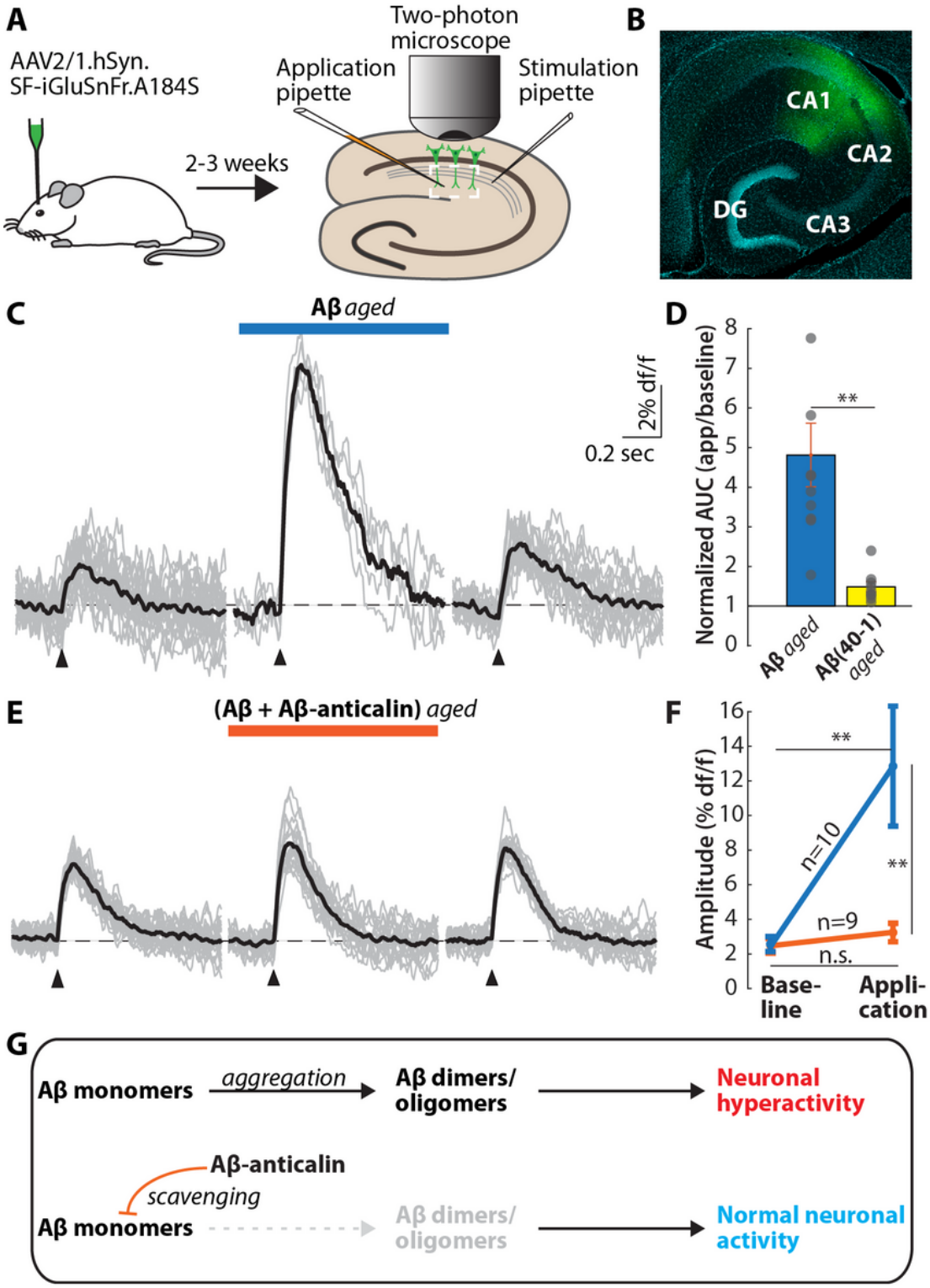

Figure 5

The Aβ-anticalin prevents Aβ-dependent synaptic dysfunctions. (**A**) Schematic of the SF-iGluSnFR-based glutamate imaging experiment. AAV-injection *in vivo* (*left*) and *in vitro* population imaging (*right*). (**B**) Representative confocal image of the SF-iGluSnFR-expressing CA1 region of a wild type mouse. SF-iGluSnFr (green) and DAPI counterstaining (cyan). DG: dentate gyrus, Ca: cornu ammonis. (**C**) Individual synaptically evoked glutamate transients (*grey*) and average (*black*) from one slice during baseline

conditions (*left*), during the application of ‘aged’ Aβ (50 μM monomer equivalent, incubated for 20 min in ACSF; *middle*) and after washout (*right*). (**D**) Area under the curve of the evoked glutamate transients during the application of ‘aged’ Aβ(1-40) (N=6 slices) or ‘aged’ reverse Aβ(40-1) (N=6), normalized to the respective AUC registered under baseline conditions. (**E**) Same as (**C**) for the application of Aβ/Aβ-anticalin (50μM Aβ monomer equivalent, incubated in ACSF containing 50μM of the Aβ-anticalin for 20 minutes). (**F**) Comparison of the amplitudes of glutamate transients before (*left*) and during (*right*) the application of 50 μM equivalent Aβ monomer, incubated for 20 min without (*blue*) or with (*orange*) Aβ-anticalin. (**G**) Schematic depicting the mechanism of action of the Aβ-anticalin. Under disease conditions, nascent Aβ monomers rapidly aggregate into toxic dimers and oligomers, which cause neuronal hyperactivity (*top*). Scavenging these monomers by the Aβ-anticalin disrupts the formation of toxic dimers/oligomers, thus preventing neuronal hyperactivation (*bottom*).

Supplementary Files

This is a list of supplementary files associated with this preprint. Click to download.

- supplement.pdf